Indonesian Journal of Physics
Vol. 33. No.1, 17 October 2022
Journal homepage: http://ijphysics.com

Compatibility of Einstein-Gauss-Bonnet Inflation Theory with Non-Minimal Derivative Coupling in the Constant-Roll

N A Adam[1*], G Hikmawan[1], F P Zen[1,2]
[1]*Theoretical Physics Division, Institut Teknologi Bandung, Jl. Ganesha 10 Bandung 40132, Indonesia*
[2]*Indonesia Center for Theoretical and Mathematical Physics (ICTMP), Jl. Ganesha 10 Bandung 40132, Indonesia*

(Received: 28 February 2022, Revised: 30 May 2022, Accepted: 11 October 2022)

Abstract

Inflation is a theory in cosmology that explains that the early universe experienced a very fast expansion in a very short time and is able to explain some cosmological problems and the presence of gravitational waves generated during the inflation period. Based on the event GW170817, it was found that $c_t^2 = 1$, which indicates that the speed of gravitational waves is nearly equal to the speed of light. This contradicts several modified theories of gravity, one of which is the Einstein-Gauss-Bonnet theory. This paper examines the compatibility of Einstein-Gauss-Bonnet inflation theory with the GW170817 phenomenon, with the addition of the non-minimal derivative coupling term and the constant-roll approach and its characteristics. The formulation of observational quantities is carried out using Horndeski theory and Effective Field Theory with ADM formalism and the calculations are done numerically. The constant values are selected in such a way that the spectral index values and tensor-scalar ratios are close to the 2018 Planck data. The results found that this theory is compatible with GW170817 with the influence of Gauss-Bonnet term and constant-roll parameter β most dominant.

Keywords: Constant-roll, Einstein-Gauss-Bonnet, GW170817, Inflation, Non-minimal derivative coupling.

INTRODUCTION

The neutron star merger that produces GW170817 provides information that gravitational wave has a speed almost the same as electromagnetic radiation that produced by itself [1]. This fact states that the speed of gravitational waves is almost the same as the speed of light ($c_t^2 = 1$). Unfortunately, this fact also contradicts some of the generalized theories of Einstein's theory of gravity that do not predict massless graviton, one of them is Einstein-Gauss-Bonnet [2].

Einstein-Gauss-Bonnet theory is the theory that is believed to be a theory that is able to explain the era of inflation and several other primordial astrophysical objects because this theory is motivated by string theory. Several studies on Gauss-Bonnet compatibility with GW170817 have been done, and one of them is by using the constant-roll evolution [3]. The constant-roll is known to enhance the non-Gaussianities features [4]. The results indicate that Gauss-Bonnet with constant-roll is compatible with GW170817 and Planck 2018 data.

Another study for this case is to add non-minimal derivative coupling (NMDC) in slow-roll evolution [5] and the results of this study also indicate that this model is compatible with GW170817 and Planck 2018 data. The presence of the NMDC allows inflationary attractors to exist and they can be used to apply a primordial phase transition model with an extended inflation scheme [6].

Those studies motivated the author to work on a gravitational wave based on the Gauss-Bonnet inflation model with NMDC on constant-roll and check its compatibility with GW170817. The presence of two arbitrary coupling functions that depend on the scalar fields makes it possible to obtain several varied solutions.

GENERAL FORMULATION OF EINSTEIN-GAUSS-BONNET INFLATION THEORY

1* Corresponding author. E-mail address: naufal.auliadam@gmail.com

WITH NON-MINIMAL DERIVATIVE COUPLING IN THE CONSTANT-ROLL

Non-minimal derivative coupled Einstein-Gauss-Bonnet theory can be described by the gravitational action

$$S = \int d^4x\sqrt{-g}\left[\frac{R}{2\kappa^2} - \frac{1}{2}(\nabla\phi)^2 + \frac{1}{8}f_1(\phi)R^2_{GB} + f_2(\phi)G_{\mu\nu}\phi^{;\mu\nu} - V(\phi)\right] \tag{1}$$

where $\kappa = \frac{1}{M_P} \equiv 1$ as gravitational constant with M_P denotes the reduced Planck mass, $V(\phi)$ is scalar potential, and $G_{\mu\nu}$ is Einstein tensor. R^2_{GB} is Gauss-Bonnet invariant that can be described as

$$R^2_{GB} = R^2 - 4R_{\alpha\beta}R^{\alpha\beta} + R_{\alpha\beta\gamma\delta}R^{\alpha\beta\gamma\delta} \tag{2}$$

with $R_{\alpha\beta}$ and $R_{\alpha\beta\gamma\delta}$ as Ricci tensor and Riemann tensor. Coupling function $f_1(\phi)$ denotes the Gauss–Bonnet coupling scalar function and $f_2(\phi)$ denotes the non-minimal derivative coupling function. By varying the gravitational action (1) we get the field equations

$$3H^2 = \frac{1}{2}\left(\dot{\phi}\right)^2 + V(\phi) - 3f_1^{(1)}(\phi)\dot{\phi}H^3 - 9f_2^{(1)}(\phi)\left(\dot{\phi}\right)^2H^2 \tag{3.a}$$

$$-2\dot{H} = \left(\dot{\phi}\right)^2 - f_1^{(1)}(\phi)\dot{\phi}H^3 + 2f_1^{(1)}(\phi)\dot{\phi}H\dot{H} + f_1^{(1)}(\phi)\ddot{\phi}H^2 + f_1^{(2)}(\phi)\left(\dot{\phi}\right)^2H^2 - 6f_2^{(1)}(\phi)\left(\dot{\phi}\right)^2H^2 + 4f_2^{(1)}(\phi)\dot{\phi}\ddot{\phi}H + 2f_2^{(1)}(\phi)\left(\dot{\phi}\right)^2\dot{H} + 2f_2^{(2)}(\phi)\left(\dot{\phi}\right)^3H \tag{3.b}$$

$$V^{(1)}(\phi) + 3H\dot{\phi} + \ddot{\phi} = 3f_1^{(1)}(\phi)H^2\left(\dot{H} + H^2\right) + 3f_2^{(2)}(\phi)\left(\ddot{\phi}\right)^2H^2 + 6f_2^{(1)}(\phi)\ddot{\phi}H^2 + 18f_2^{(1)}(\phi)\dot{\phi}H^3 + 12f_2^{(1)}(\phi)H\dot{H} \tag{3.c}$$

where $V^{(1)}(\phi)$ is the first derivative of $V(\phi)$ with respect to scalar field ϕ. Constant-roll condition provides

$$\dot{H} \lll H^2 \tag{4.a}$$

$$\frac{1}{2}\left(\dot{\phi}\right)^2 \lll V(\phi) \tag{4.b}$$

$$\ddot{\phi} = \beta H\dot{\phi} \tag{4.c}$$

with $f_1(\phi) \ll 1$ and $f_2(\phi) \ll 1$ so (3) can be simplified as

$$H^2 \simeq \frac{1}{3}V(\phi) \tag{5.a}$$

$$\dot{H} \simeq -\frac{1}{2}\left(\dot{\phi}\right)^2 \tag{5.b}$$

$$V^{(1)}(\phi) + (3+\beta)H\dot{\phi} \simeq 0. \tag{5.c}$$

The explicit aim of this paper is to calculate the observational quantities such as spectral indices and tensor-to-scalar ratio from selected models and compare them with the Planck 2018 data. The next step is to calculate the perturbation of (1) to obtain the formulation of the observational quantities. Perturbation of (1) can be formulated with ADM formalism using Horndeski theory [7]. The Lagrangian of Horndeski is defined as

$$L = \sum_{i=2}^{5} L_i, \tag{6}$$

with

$$L_2 = G_2(\phi, X), \tag{7.a}$$

$$L_3 = G_3(\phi, X)\Box\phi, \tag{7.b}$$

$$L_4 = G_4(\phi, X)R - 2G_{4X}(\phi, X)\left[(\Box\phi)^2 - \phi^{;\mu\nu}\phi_{;\mu\nu}\right] \tag{7.c}$$

$$L_4 = G_4(\phi, X)R - 2G_{4X}(\phi, X)\left[(\Box\phi)^2 - \phi^{;\mu\nu}\phi_{;\mu\nu}\right], \tag{7.d}$$

$$L_5 = G_5(\phi, X)G_{\mu\nu}\phi^{;\mu\nu} + \frac{1}{3}G_{5X}(\phi, X)\left[(\Box\phi)^3 - 3(\Box\phi)\phi_{;\mu\nu}\phi^{;\mu\nu} + 2\phi_{;\mu\nu}\phi^{;\mu\sigma}\phi^{;\nu}_{;\sigma}\right]. \tag{7.e}$$

Here $G_i(i = 2,3,4,5)$ in (5) are functions that depends on scalar field ϕ and its kinetic energy $X = g^{\mu\nu}\partial_\mu\phi\partial_\nu$ with $G_{iX} \equiv \partial G_i/\partial X$ and $G_{i\phi} \equiv \partial G_i/\partial\phi$ are partial derivatives of G_i. According to (7), (1) can be rewritten as

$$G_2 = -\frac{X}{2} - V(\phi) + \frac{1}{4}f_1^{(4)}(\phi)X^2\left[3 - ln\left(-\frac{X}{2}\right)\right], \tag{8.a}$$

$$G_3 = -\frac{1}{4}f_1^{(3)}(\phi)X\left[7 - 3\,ln\left(-\frac{X}{2}\right)\right], \tag{8.b}$$

$$G_4 = \frac{1}{2} - \frac{1}{2}f_1^{(2)}(\phi)X\left[2 - ln\left(-\frac{X}{2}\right)\right], \tag{8.c}$$

$$G_5 = -\frac{1}{2}f_1^{(1)}(\phi)\,ln\left(-\frac{X}{2}\right) + f_2(\phi). \tag{8.d}$$

General slow-roll parameter is defined as

$$\epsilon \equiv -\frac{\dot{H}}{H^2} \tag{9}$$

and constant-roll condition provides another slow-roll parameter as

$$\beta = -\frac{\ddot{\phi}}{H\dot{\phi}} \tag{10}$$

which is also a constant-roll parameter. ADM formalism also provides four additional slow-roll parameters as

$$\delta_{Q_s} \equiv \frac{\dot{Q}_s}{HQ_s}, \tag{11.a}$$

$$\delta_{Q_t} \equiv \frac{\dot{Q}_t}{HQ_t}, \tag{11.b}$$

$$\delta_{c_s} \equiv \frac{\dot{c}_s}{Hc_s}, \tag{11.c}$$

$$\delta_{c_t} \equiv \frac{\dot{c}_t}{Hc_t} \tag{11.d}$$

with

$$Q_s \equiv \frac{2L_{\mathcal{S}}}{3\mathcal{W}^2}(9\mathcal{W}^2 + 8L_{\mathcal{S}}w), \tag{12.a}$$

$$c_s^2 \equiv \frac{2}{Q_s}\left(\dot{\mathcal{M}} + H\mathcal{M} - \mathcal{E}\right), \tag{12.b}$$

$$Q_t \equiv \frac{L_{\mathcal{S}}}{2}, \tag{12.c}$$

$$c_t^2 \equiv \frac{\mathcal{E}}{L_{\mathcal{S}}} \tag{12.d}$$

where

$$L_{\mathcal{S}} = G_4 - 2XG_{4X} - H\dot{\phi}XG_{5X} - \frac{1}{2}XG_{5\phi}, \tag{13.a}$$

$$\mathcal{E} = G_4 + \frac{1}{2}XG_{5\phi} - XG_{5X}\ddot{\phi}, \tag{13.b}$$

$$\begin{aligned} w = &-18H^2G_4 + 3(XG_{2X} + 2X^2G_{2XX}) \\ &- 18H\dot{\phi}(2XG_{3X} + X^2G_{3XX}) \\ &- 3X\left(G_{3\phi} + XG_{3\phi X}\right) \\ &+ 18H^2(7XG_{4X} + 16X^2G_{4XX} \\ &+ 4X^3G_{4XXX}) \\ &- 18H\dot{\phi}\left(G_{4\phi} + 5XG_{4\phi X}\right. \\ &+ 2X^2G_{4\phi XX}\left.\right) \\ &+ 6H^3\dot{\phi}(15XG_{5X} + 13X^2G_{5XX} \\ &+ 2X^3G_{5XXX}) \\ &+ 9H^2X\left(6G_{5\phi} + 9XG_{5\phi X}\right. \\ &+ 2X^2G_{5\phi XX}\left.\right), \end{aligned} \tag{13.c}$$

$$\begin{aligned} \mathcal{W} = &\ 4HG_4 + 2\dot{\phi}XG_{3X} - 16H(XG_{4X} + X^2G_{4XX}) \\ &+ 2\dot{\phi}\left(G_{4\phi} + 2XG_{4\phi X}\right) \\ &- 2H^2\dot{\phi}(5XG_{5X} + 2X^2G_{5XX}) \\ &- 2HX\left(3G_{5\phi} + 2XG_{5\phi X}\right), \end{aligned} \tag{13.d}$$

$$\mathcal{M} = \frac{4L_S^2}{\mathcal{W}}. \tag{13.e}$$

Equations (11) came from our assumption about small variations of (12) since Hubble parameter H is nearly constant during inflation. The conditions for the avoidance of the ghost and Laplacian instability are given by $L_S > 0$ and $\mathcal{E} > 0$ for tensor perturbation cases and $Q_s > 0$ and $c_s^2 > 0$ for scalar perturbation cases [8]. Observational quantities such as spectral indices and tensor-to-scalar ratios can be formulated as

$$n_s = 1 - 2\epsilon - \delta_{Q_s} - 3\delta_{c_s}, \tag{14.a}$$

$$n_t = -2\epsilon - \delta_{Q_t} - 3\delta_{c_t}, \tag{14.b}$$

$$r = 4\frac{Q_s c_s^3}{Q_t c_t^3} \tag{14.c}$$

with n_s as scalar spectral index, n_t as tensor spectral index, and r as tensor-to-scalar ratio. Both of spectral indices n_s and n_t are the parameter that describes the nature of primordial density perturbations, where n_s represents scalar fluctuations, n_t represents tensor fluctuations, and r represents ratio of their power spectra. We refer readers to [7] for how to derive (11)-(14) and more detailed explanations. Condition $c_t^2 = 1$ can be implemented to (1), (13.a), and (13.b) so we get

$$\dot{\phi} = \frac{f_1^{(1)}(\phi)(1-\beta)H}{f_1^{(2)}(\phi) - 2f_2^{(1)}(\phi)}. \tag{15}$$

The value of scalar field ϕ in this paper uses the initial value of scalar field ϕ_i, which is the value of the scalar field at the beginning of inflation. This quantity can be formulated from the e-foldings number N, defined as

$$N = \int_{\phi_i}^{\phi_f} \frac{H}{\dot{\phi}} d\phi \tag{16}$$

where ϕ_f is the final value of scalar field which is the value of the scalar field at the end of inflation that can be formulated by equating slow-roll parameter (9) $\epsilon = 1$.

SPECIFIC MODELS OF EINSTEIN-GAUSS-BONNET INFLATION THEORY WITH NON-MINIMAL DERIVATIVE COUPLING IN THE CONSTANT-ROLL

In this paper, we construct eight models based on variations of $f_1(\phi)$ and $f_2(\phi)$. Derivation of equations is done analytically by hand, while calculations and contour plots are done numerically by MATLAB.

Model I: Linear $f_1(\phi)$ and Quadratic $f_2(\phi)$

In this model we defined

$$f_1(\phi) = \lambda\phi, \tag{17.a}$$

$$f_2(\phi) = \sigma\phi^2 \tag{17.b}$$

where λ and σ are the arbitrary constants for coupling functions. We apply (17) to (5.c) and (15) so the scalar potential can be written as

$$V(\phi) = V_0\, exp\left[\frac{(3+\beta)(1-\beta)\lambda}{12\sigma}\right] \tag{18}$$

where V_0 is the constant for scalar potential. Next, we use $\epsilon = 1$ from (5.a), (5.b), and (9) to find the equation of the final value of a scalar field,

$$\phi_f = \pm\frac{\lambda(1-\beta)}{4\sqrt{2}\sigma} \tag{19}$$

where we always use the positive value of scalar fields. The equation of the initial value of a scalar field can be derived from (16) so it can be written as

$$\phi_i = \sqrt{\phi_f^2 + \frac{N(1-\beta)\lambda}{2\sigma}}. \tag{20}$$

Furthermore, the spectral indices and tensor-to-scalar ratio can be calculated using the equations that have been derived previously. Calculations are performed numerically using MATLAB. The constant values are made in such a way that the scalar spectral index and tensor-scalar ratio values are close to the values in the 2018 Planck data as [9]

$$n_s = 0.9649 \pm 0.0042, \tag{21.a}$$

$$r < 0.064. \tag{21.b}$$

Constant values and calculation results for this model can be seen in Table 1 and the contour plot can be seen in Fig. 1-2.

Table 1. Constant values and calculation results of Model I.

Quantity	Value
λ	-8×10^{-7}
σ	-2×10^{-6}
β	0.01
N	60
V_0	20
ϕ_f	0.07000
ϕ_i	3.44745
n_s	0.96489
n_t	−0.00329
r	0.02633
$\dot{\phi}^2$	0.08372
$V(\phi)$	76.14935
$\dot{H}$	−0.04186
H^2	25.38312
$f_1(\phi)$	-2.75×10^{-6}
$f_2(\phi)$	-2.37×10^{-5}
L_S	0.5
$\mathcal{E}$	0.5
Q_s	0.00165
c_s^2	0.99784

It can be seen in Table 1 that the value of the scalar field decreases. In addition, $\dot{H} \ll H^2$ and $\dot{\phi}^2/2 \ll V(\phi)$ so that it satisfies the condition of constant-roll. The values of $L_S, \mathcal{E}, Q_s, c_s^2 > 0$, so that the conditions for avoiding *ghost* and Laplacian instability are met and the value of the scalar propagation speed is close to the speed of light ($c_s^2 \approx 1$).

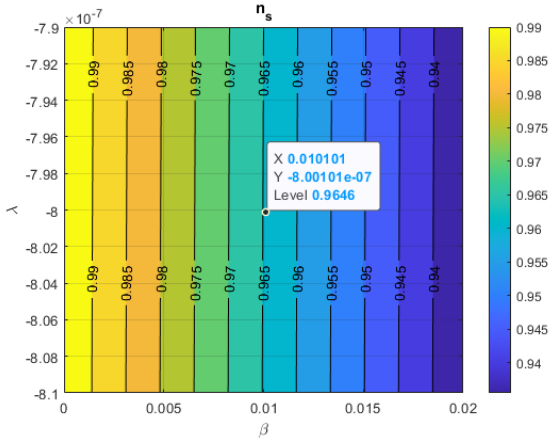

Fig. 1. Contour plots of n_s on model I.

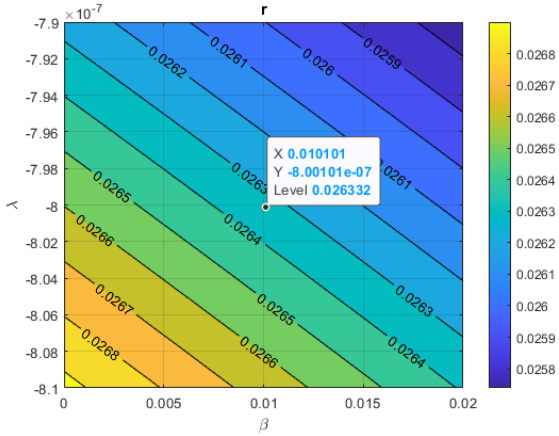

Fig. 2. Contour plots of r on model I.

We have provided two contour graphs for the values of n_s and r by selecting the constant-roll β as the x coordinates and the Gauss-Bonnet coupling constants λ as the y coordinates. This selection is based on the frequent occurrence of the two constants in the equations. It can be seen that the contour lines of n_s are drawn vertically indicating that its value is more influenced by β.

Model II: Linear $f_1(\phi)$ and Qubic $f_2(\phi)$

In this model we defined

$$f_1(\phi) = \lambda\phi, \tag{22.a}$$

$$f_2(\phi) = \sigma\phi^3. \tag{22.b}$$

Derivation of the equations for this model is done in the same way as the previous model. The scalar potential can be written as

$$V(\phi) = V_0\, exp\left[-\frac{(3+\beta)(1-\beta)}{18\phi}\right]. \tag{23}$$

The equation of the final value of a scalar field is

$$\phi_f = \sqrt{\pm\frac{\lambda(1-\beta)}{6\sqrt{2}\sigma}} \tag{24}$$

so the equation of the initial value of a scalar field can be written as

$$\phi_i = \frac{\lambda(1-\beta)\phi_f}{\lambda(1-\beta) - 6\sigma N\phi_f}. \tag{25}$$

Constant values and calculation results for this model can be seen in Table 2 and the contour plot can be seen in Fig, 3-4.

Table 2. Constant values and calculation results of Model II.

Quantity	Value
λ	-1×10^{-7}
σ	-4.25×10^{-12}
β	0.01
N	60
V_0	25
ϕ_f	52.39502
ϕ_i	2.75388×10^{2}
n_s	0.96453
n_t	−0.00262
r	0.02095
$\dot{\phi}^2$	0.02182
$V(\phi)$	24.98497
$\dot{H}$	−0.01091
H^2	8.32832
$f_1(\phi)$	-2.75388×10^{-5}
$f_2(\phi)$	-8.87615×10^{-5}
L_S	0.5
$\mathcal{E}$	0.5
Q_s	0.00131
c_s^2	0.99974

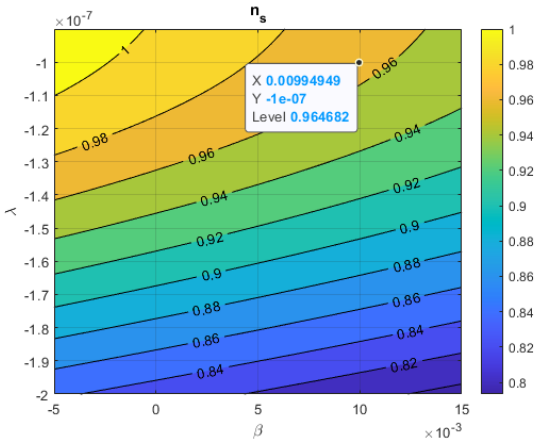

Fig. 3. Contour plots of n_s on model II.

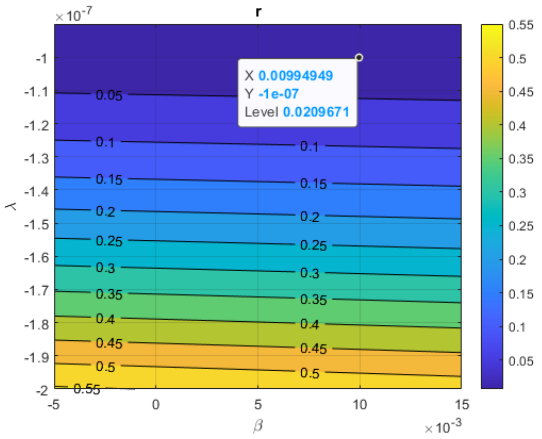

Fig. 4. Contour plots of r on model II.

It can be seen in Table 2 that the value of the scalar field in this model is increases and the rest of the values satisfy the condition for constant-roll and avoiding *ghost* and Laplacian instability. Fig. 2-3 show that it is possible to apply the slow-roll condition ($\beta = 0$) with some minor changes in λ and the contour lines of r are slightly horizontal indicating that r is more influenced by λ.

Model III: Quadratic $f_1(\phi)$ and Zero $f_2(\phi)$

In this model we defined

$$f_1(\phi) = \lambda\phi, \tag{26.a}$$

$$f_2(\phi) = 0. \tag{26.b}$$

Derivation of the equations for this model is done in the same way as the previous model. The scalar potential can be written as

$$V(\phi) = V_0\, exp\left[-\frac{(3+\beta)(1-\beta)}{6}\phi^2\right]. \tag{27}$$

The equation of the final value of a scalar field is

$$\phi_f = \pm\frac{\sqrt{2}}{(1-\beta)} \tag{28}$$

so the equation of the initial value of a scalar field can be written as

$$\phi_i = \phi_f\left[exp\big((1-\beta)N\big)\right]^{-1}. \tag{29}$$

Constant values and calculation results for this model can be seen in Table 3 and the contour plot can be seen in Fig. 5-6.

Table 3. Constant values and calculation results of Model III.

Quantity	Value
λ	-1.09
σ	0
β	0.92
N	60
V_0	0.09
ϕ_f	17.67766
ϕ_i	0.14548
n_s	0.96433
n_t	-2.48386×10^{-5}
r	0.00108
$\dot{\phi}^2$	4.05923×10^{-6}
$V(\phi)$	0.08990
$\dot{H}$	-2.02961×10^{-6}
H^2	0.02996
$f_1(\phi)$	-0.02307
$f_2(\phi)$	0
L_S	0.5
$\mathcal{E}$	0.5
Q_s	6.77454×10^{-5}
c_s^2	0.99988

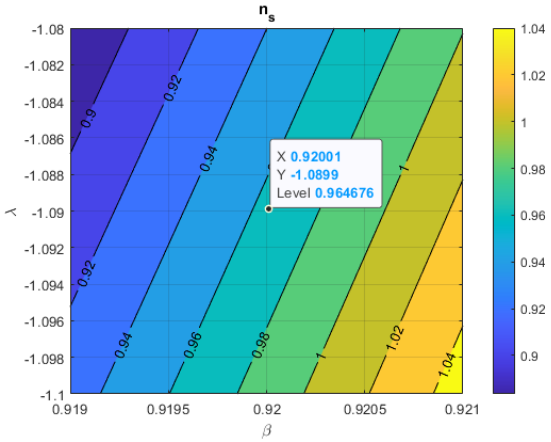

Fig. 5. Contour plots of n_s on model III.

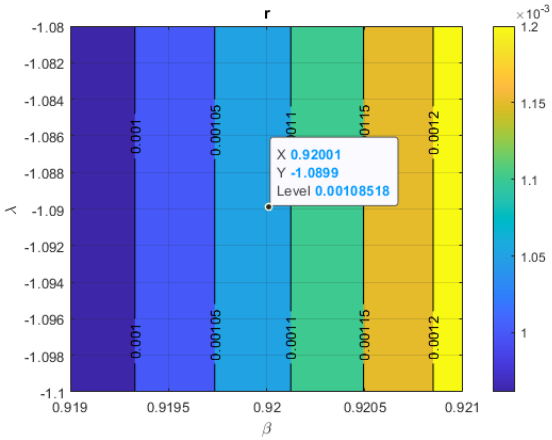

Fig. 6. Contour plots of r on model III.

It can be seen in Table 3 that the value of the scalar field in this model is increases and the rest of the values satisfy the condition for constant-roll and avoiding *ghost* and Laplacian instability. Fig. 5-6 show the contour lines of r are slightly vertical indicating that r is more influenced by β. Since $\beta > 0.9$, it might be impossible to apply a slow-roll condition for this model.

Model IV: Quadratic $f_1(\phi)$ and Linear $f_2(\phi)$

In this model we defined

$$f_1(\phi) = \lambda\phi^2, \tag{30.a}$$

$$f_2(\phi) = \sigma\phi. \tag{30.b}$$

Derivation of the equations for this model is done in the same way as the previous model. The scalar potential can be written as

$$V(\phi) = V_0\, exp\left[-\frac{(3+\beta)(1-\beta)\lambda}{6(\lambda-\sigma)}\phi^2\right].$$

(31)

The equation of the final value of a scalar field is

$$\phi_f = \pm\frac{\sqrt{2}(\lambda-\sigma)}{\lambda(1-\beta)} \tag{32}$$

so the equation of the initial value of a scalar field can be written as

$$\phi_i = \phi_f\left[exp\left(\frac{(1-\beta)\lambda N}{\lambda-\sigma}\right)\right]^{-1}. \tag{33}$$

Constant values and calculation results for this model can be seen in Table 4 and the contour plot can be seen in Fig. 7-8.

Table 4. Constant values and calculation results of Model IV.

Quantity	Value
λ	-0.005×10^{-5}
σ	0.01×10^{-4}
β	6.5×10^{-3}
N	60
V_0	0.5
ϕ_f	29.89278
ϕ_i	1.74900
n_s	0.96424
n_t	−0.00684
r	0.05476
$\dot{\phi}^2$	0.00106
$V(\phi)$	0.46502
$\dot{H}$	-5.30643×10^{-4}
H^2	0.15500
$f_1(\phi)$	-1.52950×10^{-7}
$f_2(\phi)$	1.74900×10^{-6}
L_S	0.5
$\mathcal{E}$	0.5
Q_s	0.00342
c_s^2	0.99985

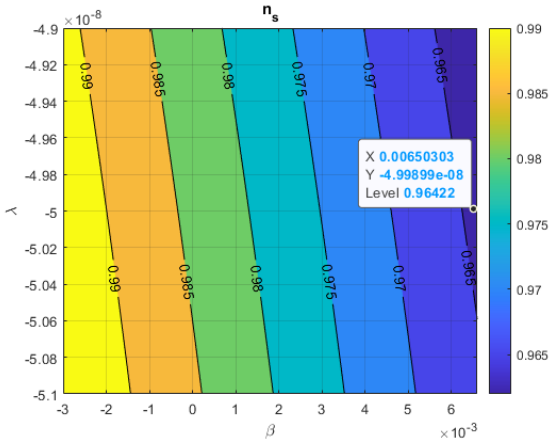

Fig. 7. Contour plots of n_s on model IV.

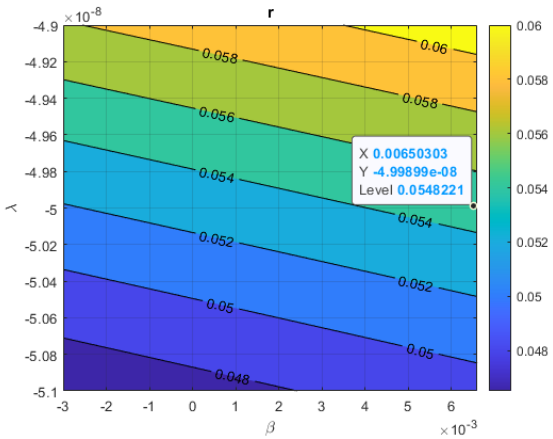

Fig. 8. Contour plots of r on model IV.

It can be seen in Table 4 that the value of the scalar field in this model is increases and the rest of the values satisfy the condition for constant-roll and avoiding *ghost* and Laplacian instability. Fig. 7-8 show that the contour lines of n_s are slightly vertical indicating that its value is more influenced by β while the contour lines of r are slightly horizontal indicating that its value is more influenced by λ. Since the values of n_s and r are rapidly changing due to the changes of values of β and λ, it might be impossible to apply a slow-roll condition for this model.

Model V: Quadratic $f_1(\phi)$ and Quadratic $f_2(\phi)$

In this model we defined

$$f_1(\phi) = \lambda\phi^2, \tag{34.a}$$

$$f_2(\phi) = \sigma\phi^2. \tag{34.b}$$

Derivation of the equations for this model is done in the same way as the previous model. The scalar potential can be written as

$$V(\phi) = \left[\frac{\lambda - 2\sigma\phi}{\lambda}\right]^m exp(n\phi) \tag{35}$$

where

$$m = \frac{\lambda^2}{12\sigma^2}(3+\beta)(1-\beta), \tag{36.a}$$

$$n = \frac{\lambda}{6\sigma}(3+\beta)(1-\beta). \tag{36.b}$$

The equation of the final value of a scalar field is

$$\phi_f = \pm\frac{\sqrt{2}}{(1-\beta) \pm \frac{2\sqrt{2}\sigma}{\lambda}}, \tag{37}$$

so the equation of the initial value of a scalar field can be written as

$$\phi_i = \frac{q \pm \sqrt{q^2 - 4p}}{2p} \tag{38}$$

with

$$p = \frac{2\sigma^2}{\lambda^2}, \tag{39.a}$$

$$q = \frac{1}{\phi_f} \cdot exp\left[N(1-\beta) + \frac{2\sigma}{\lambda}\phi_f\right] - \frac{2\sigma}{\lambda}. \tag{39.b}$$

Constant values and calculation results for this model can be seen in Table 5 and the contour plot can be seen in Fig. 9-10.

Table 5. Constant values and calculation results of Model V.

Quantity	Value
λ	-7.01×10^{-2}
σ	-0.468×10^{-5}
β	0.9503
N	60
V_0	8.131×10^{-1}
ϕ_f	28.34729
ϕ_i	1.43180
n_s	0.96499
n_t	-0.00144
r	0.04089
$\dot{\phi}^2$	0.00128
$V(\phi)$	0.76033
$\dot{H}$	-6.41954×10^{-4}
H^2	0.25344
$f_1(\phi)$	-0.14371
$f_2(\phi)$	-9.59434×10^{-6}
L_S	0.5
$\mathcal{E}$	0.5
Q_s	0.00255
c_s^2	0.99859

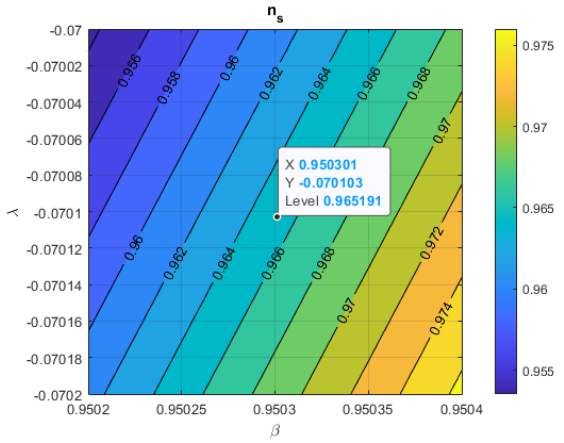

Fig. 9. Contour plots of n_s on model V.

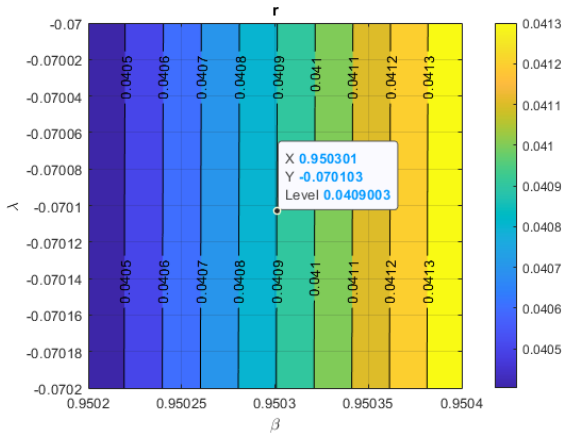

Fig. 10. Contour plots of r on model V.

It can be seen in Table 5 that the value of the scalar field in this model is increases and the rest of the values satisfy the condition for constant-roll and avoiding *ghost* and Laplacian instability. Fig. 9-10 show that the contour lines of r are vertical indicating that its value is more influenced by β. Since $\beta > 0.9$, it might be impossible to apply a slow-roll condition for this model.

Model VI: Quadratic $f_1(\phi)$ and Qubic $f_2(\phi)$

In this model we defined

$$f_1(\phi) = \lambda\phi^2, \tag{40.a}$$

$$f_2(\phi) = \sigma\phi^3. \tag{40.b}$$

Derivation of the equations for this model is done in the same way as the previous model. The scalar potential can be written as

$$V(\phi) = V_0\left[1 - \frac{3\sigma\phi^2}{\lambda}\right]^{\frac{\lambda}{9\sigma}(3+\beta)(1-\beta)}. \tag{41}$$

The equation of the final value of a scalar field is

$$\phi_f = \frac{-n \pm \sqrt{n^2 - 4m}}{2m} \tag{42}$$

where

$$m = \frac{3\sigma}{\lambda}, \tag{43.a}$$

$$n = \frac{(1-\beta)}{\sqrt{2}} \tag{43.b}$$

so the equation of the initial value of a scalar field can be written as

$$\phi_i = \frac{q \pm \sqrt{q^2 - 4p}}{2p} \tag{44}$$

where

$$p = \frac{3\sigma}{2\lambda}, \tag{45.a}$$

$$q = \frac{1}{\phi_f} \cdot exp\left[N(1-\beta) + \frac{3\sigma}{2\lambda}\phi_f^2\right]. \tag{45.b}$$

Constant values and calculation results for this model can be seen in Table 6 and the contour plot can be seen in Fig. 11-12.

Table 6. Constant values and calculation results of Model VI.

Quantity	Value
λ	-0.05
σ	1.25×10^{-3}
β	0.857
N	60
V_0	4
ϕ_f	4.38729
ϕ_i	0.00169
n_s	0.96401
n_t	-3.97625×10^{-9}
r	4.70190×10^{-7}
$\dot{\phi}^2$	7.84277×10^{-8}
$V(\phi)$	3.99999
$\dot{H}$	-3.92138×10^{-8}
H^2	1.33333
$f_1(\phi)$	-1.43823×10^{-7}
$f_2(\phi)$	6.09816×10^{-12}
L_S	0.5
$\mathcal{E}$	0.5
Q_s	2.94104×10^{-8}
c_s^2	0.99946

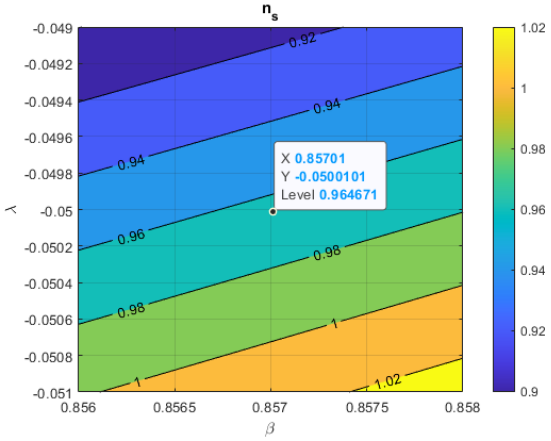

Fig. 11. Contour plots of n_s on model VI.

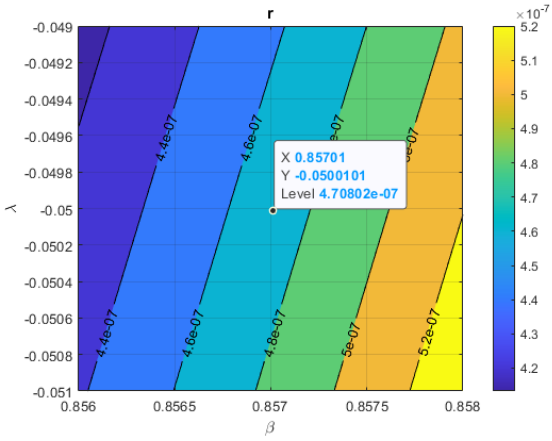

Fig. 12. Contour plots of r on model VI.

It can be seen in Table 6 that the value of the scalar field in this model is increases and the rest of the values satisfy the condition for constant-roll and avoiding *ghost* and Laplacian instability. Fig. 11-12 show that the contour lines of n_s are slightly horizontal indicating that its value is more influenced by λ while the contour lines of r are slightly vertical indicating that its value is more influenced by β. Since $\beta > 0.8$, it might be impossible to apply a slow-roll condition for this model.

Model VII: Qubic $f_1(\phi)$ and Linear $f_2(\phi)$

In this model we defined

$$f_1(\phi) = \lambda\phi^3, \tag{46.a}$$

$$f_2(\phi) = \sigma. \tag{46.b}$$

Derivation of the equations for this model is done in the same way as the previous model. The scalar potential can be written as

$$V(\phi) = V_0\left(1 - \frac{6\lambda\phi}{\sigma}\right)^{-m} exp(-n) \tag{47}$$

with

$$m = \frac{\sigma^2(3+\beta)(1-\beta)}{216\lambda^2}, \tag{48.a}$$

$$n = \frac{(3+\beta)(1-\beta)(\sigma+3\lambda\phi)\phi}{36\lambda}. \tag{48.b}$$

The equation of the final value of a scalar field is

$$\phi_f = \frac{q \pm \sqrt{q^2 - 4po}}{2p} \tag{49}$$

with

$$p = 3\lambda, \tag{50.a}$$

$$q = \frac{6\sqrt{2}}{(1-\beta)}, \tag{50.b}$$

$$o = \frac{2\sqrt{2}\sigma}{(1-\beta)} \tag{50.c}$$

so the equation of the initial value of a scalar field can be written as

$$\phi_i = \frac{1 \pm \sqrt{1-4tu}}{2t} \tag{51}$$

with

$$t = \frac{1}{\phi_f} exp\left[\frac{(1-\beta)N}{2} - \frac{\sigma}{6\lambda\phi_f}\right], \tag{52.a}$$

$$u = \frac{\sigma}{6\lambda}. \tag{25.b}$$

Constant values and calculation results for this model can be seen in Table 7 and the contour plot can be seen in Fig. 13-14.

Table 7. Constant values and calculation results of Model VII.

Quantity	Value
λ	-0.14565
σ	0.00001
β	0.85
N	60
V_0	0.0001
ϕ_f	18.85620
ϕ_i	0.20948
n_s	0.96481
n_t	-2.46782×10^{-4}
r	0.00195
$\dot{\phi}^2$	8.20907×10^{-9}
$V(\phi)$	9.97890×10^{-5}
$\dot{H}$	-4.10453×10^{-9}
H^2	3.32630×10^{-5}
$f_1(\phi)$	-0.00133
$f_2(\phi)$	2.09484×10^{-6}
L_s	0.5
$\mathcal{E}$	0.5
Q_s	1.23375×10^{-4}
c_s^2	0.99263

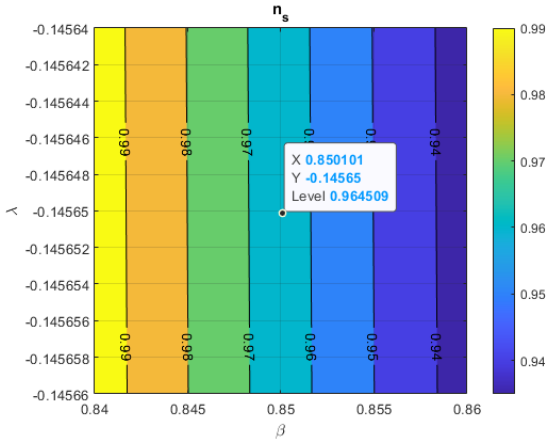

Fig. 13. Contour plots of n_s on model VII.

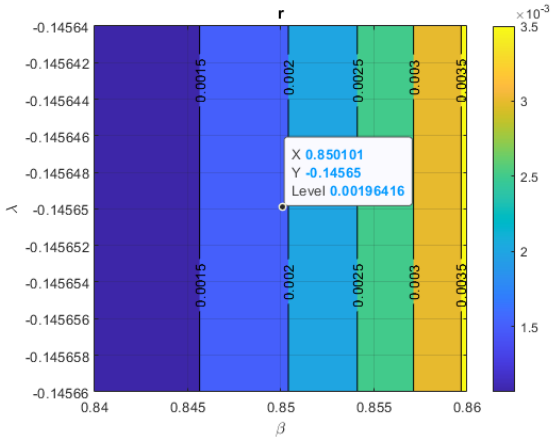

Fig. 14. Contour plots of r on model VII.

It can be seen in Table 7 that the value of the scalar field increases, and the rest of the values satisfy the condition for constant-roll and avoiding *ghost* and Laplacian instability. Fig. 13-14 show that the contour lines of both n_s and r are vertical indicating that their value is more influenced by β. Since $\beta >$ 0.8, it might be impossible to apply a slow-roll condition for this model.

Model VIII: Qubic $f_1(\phi)$ and Quadratic $f_2(\phi)$

In this model we defined

$$f_1(\phi) = \lambda\phi^3, \tag{53.a}$$

$$f_2(\phi) = \sigma\phi^2. \tag{53.b}$$

Derivation of the equations for this model is done in the same way as the previous model. The scalar potential can be written as

$$V(\phi) = V_0\, exp\left[-\frac{(3+\beta)(1-\beta)\lambda}{2(6\lambda-4\sigma)}\phi^2\right]. \tag{54}$$

The equation of the final value of a scalar field is

$$\phi_f = \pm\frac{\sqrt{2}(6\lambda-4\sigma)}{3\lambda(1-\beta)} \tag{55}$$

so the equation of the initial value of a scalar field can be written as

$$\phi_i = \phi_f\left[exp\left(\frac{3(1-\beta)\lambda N}{6\lambda-4\sigma}\right)\right]^{-1}. \tag{56}$$

Constant values and calculation results for this model can be seen in Table 8 and the contour plot can be seen in Fig. 15-16.

Table 8. Constant values and calculation results of Model VIII.

Quantity	Value
λ	-0.007×10^{-5}
σ	0.01×10^{-4}
β	6.5×10^{-3}
N	60
V_0	0.5
ϕ_f	29.96057
ϕ_i	1.76426
n_s	0.96467
n_t	−0.00693
r	0.05543
$\dot{\phi}^2$	0.00107
$V(\phi)$	0.46451
$\dot{H}$	-5.36910×10^{-4}
H^2	0.15483
$f_1(\phi)$	-3.84403×10^{-7}
$f_2(\phi)$	3.11262×10^{-6}
L_S	0.5
$\mathcal{E}$	0.5
Q_s	0.00346
c_s^2	0.99949

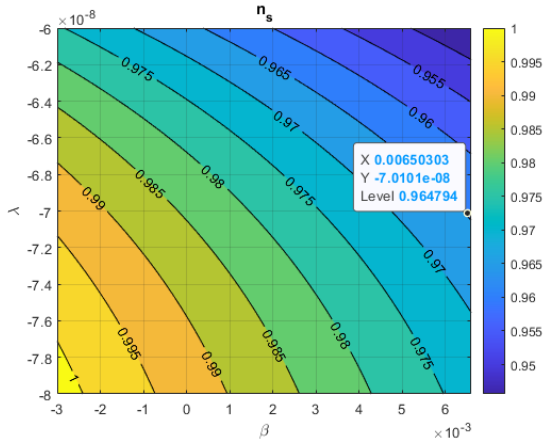

Fig. 15. Contour plots of n_s on model VIII.

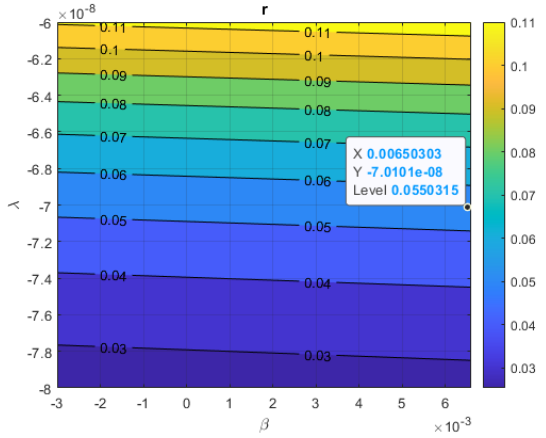

Fig. 16. Contour plots of r on model VIII.

It can be seen in Table 8 that the value of the scalar field increases, and the rest of the values satisfy the condition for constant-roll and avoiding *ghost* and Laplacian instability. Fig. 15-16 show that the contour lines of r are slightly horizontal indicating that its value is more influenced by λ. Since the values of n_s and r are rapidly changing due to the changes of values of β and λ, it might be impossible to apply a slow-roll condition for this model.

DISCUSSION

We have analyzed eight models containing variations of the Gauss-Bonnet coupling with the non-minimal derivative coupling. We start the analysis using model I because linear Gauss-Bonnet coupling with linear non-minimal derivative coupling cannot generate ϕ_f when applied to $\epsilon = 1$ and from equation (15) it can be seen that Gauss-Bonnet coupling function cannot be in constant or linear function alone without non-minimal derivative coupling.

The constant values λ, σ, β, and V_0 listed in Table (1)-(8) are "fitting" values with the values of n_s and r listed in (21). There is no definite reference regarding the value of these constants, so any value will be accepted as long as the conditions (21) are met. In addition, these values must also meet the slow-roll conditions (5) and the conditions for avoiding *ghost* and Laplacian instability. The scalar propagation speed also has the condition $c_s^2 < 1$ in order not to violate the theory of relativity and constant-roll has the condition $\beta \neq 1$ because otherwise the universe would be inflated forever (eternal inflation). We only choose $\beta \to 0$ or $\beta \to 1$ in our models.

We started the analysis with model I and model II. Both models have linear Gauss-Bonnet coupling with different non-minimal derivative coupling. The effect of non-minimal derivative coupling on linear Gauss-Bonnet coupling gives a decrease in scalar field evolution, with the higher rank of Non-minimal derivative coupling giving a larger gap.

Model III with Non-minimal zero derivative coupling gives an increase in scalar field evolution. The effect of non-minimal derivative coupling on quadratic Gauss-Bonnet coupling can be seen in Model IV-VI. Model IV with linear non-minimal derivative coupling increases the gap in the scalar field compared to model III. However, Model V-VI narrows that gap again. We chose the quadratic Gauss-Bonnet coupling as the basis for most models because it is believed to be able to provide a solution for inflation [10-12]. We can hypothesize that the effect of non-minimal derivative coupling generally reduces the scalar field gap for models that already have increased scalar field evolution, although we need to analyze more deeply for quadratic Gauss-Bonnet coupling especially for cases such as model III and model V because both models have higher values of Gauss-Bonnet coupling compared to other models.

The effect of non-minimal derivative coupling on cubic Gauss-Bonnet coupling can be seen in Model VII-VIII. Both models give an increase in scalar field evolution, with the higher rank of non-minimal derivative coupling giving a larger gap. We have also analyzed a model with a cubic Gauss-Bonnet coupling without non-minimal derivative coupling (which we do not present in this paper) and we find that the model has a larger gap in scalar field evolution compared to model VII and model VIII. We hypothesize that the effect of non-minimal derivative coupling may be different for each Gauss-Bonnet coupling, depending on the rank of the couplings. This hypothesis can be proven by model IV and model VIII. Both models have similar

constant values, the same rank difference, and an increasing scalar field evolution with similar values.

CONCLUSION

We have analyzed the compatibility of Einstein-Gauss-Bonnet inflation theory with non-minimal derivative coupling in the constant-roll case for event GW170817. We begin the analysis by deriving field equations from Lagrangian and its perturbations using ADM formalism and Horndeski theory. We also use the approximation $c_t^2 = 1$ which indicates that the speed of the gravitational wave GW170817 is almost the same as the speed of light.

We find that the Gauss-Bonnet coupling $f_1(\phi)$ and its derivatives with respect to scalar field ϕ and constant-roll parameter β appear frequently in the formulation so that it greatly affects the calculations. However, the Gauss-Bonnet coupling cannot be a constant or a linear function without a non-minimal derivative coupling because it cannot produce a scalar field.

We selected eight models in this paper and the constant values we are using are "fitting" values with the values of n_s and r listed in Planck 2018 data. We find that the evolution of the scalar field is affected by the rank of the Gauss-Bonnet coupling. Linear Gauss-Bonnet coupling produces a decreasing scalar field evolution and their higher rank produces an increasing scalar field evolution. Non-minimal derivative coupling affects its gap.

Further study can be carried out with more diverse variations of the coupling function. In addition, the MCMC (Markov Chain Monte Carlo) method can also be used to obtain more diverse constant values so that the calculations are more accurate and precise on Planck 2018 data.

REFERENCES

[1] Abbott B P *et al.*, Multi-messenger Observations of a Binary Neutron Star Merger, *The Astrophysical Journal*, **848**, L12, 2017.
[2] Odintsov S and Oikonomou V, Inflationary phenomenology of Einstein Gauss-Bonnet gravity compatible with GW170817, *Physics Letters B*, **797**, 134874, 2019.
[3] Odintsov S *et al.*, GW170817-compatible Constant-roll Einstein-Gauss-Bonnet Inflation and Non-Gaussianities, *Physics of the Dark Universe*, **30**, 100718, 2020.
[4] Odintsov S D and Oikonomou V K, Constant-roll k-inflation dynamics, *Classical and Quantum Gravity*, **37**, 025003, 2019.
[5] Oikonomou V K and Fronimos F P, Reviving non-minimal Horndeski-like theories after GW170817: kinetic coupling corrected Einstein–Gauss–Bonnet inflation, *Classical and Quantum Gravity*, **38**, 035013, 2020.
[6] Gumjudpai B and Rangdee P, Non-minimal derivative coupling gravity in cosmology, *General Relativity and Gravitation*, **47**, 140, 2015.
[7] Tsujikawa S, Modifications of Einstein's Theory of Gravity at Large Distances, Springer, Cham, 97, 2015.
[8] Gleyzes J *et al.*, Essential building blocks of dark energy, *Journal of Cosmology and Astroparticle Physics*, **2013**, 025, 2013.
[9] Akrami Y *et al.*, Planck 2018 results. X. Constraints on inflation, *Astronomy & Astrophysics*, **641**, A10, 2020.
[10] Kanti P, Gannouji R, and Dadhich N, Early-time cosmological solutions in Einstein-scalar-Gauss-Bonnet theory, *Phys. Rev. D*, **92**, 083524, 2015.
[11] Kanti P, Gannouji R, and Dadhich N, Gauss-Bonnet inflation, *Phys. Rev. D*, **92**, 041302, 2015.
[12] Hikmawan G *et al.*, Comment on "Gauss-Bonnet inflation", *Phys. Rev. D*, **93**, 068301, 2016.